Engineering Fracture Mechanics 282 (2023) 109173

Contents lists available at ScienceDirect

Engineering Fracture Mechanics

journal homepage: www.elsevier.com/locate/engfracmech

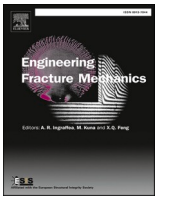

A fatigue limit evaluation method based on plastic strain incremental energy dissipation theory

Ruili Zu [a], Yingbin Zhu [b], Xianfu Huang [c], Yao Huang [a], Yizhou Zhou [d], Jiaye Zhao [e], Zhanwei Liu [a,*]

[a] School of Aerospace Engineering, Beijing Institute of Technology, Beijing 100081, People's Republic of China
[b] State Key Laboratory of Polymer Physics and Chemistry, Changchun Institute of Applied Chemistry, Chinese Academy of Sciences, Changchun 130022, People's Republic of China
[c] State Key Laboratory of Nonlinear Mechanics, Institute of Mechanics, Chinese Academy of Sciences, Beijing 100190, People's Republic of China
[d] Institute of Metal Research, Chinese Academy of Sciences, Shenyang 110016, People's Republic of China
[e] Institute of Flexible Electronics Technology of THU, Zhejiang 314006, People's Republic of China

ARTICLE INFO

Keywords:
Fatigue limit
Plastic strain incremental energy dissipation theory
Infrared thermal imaging
Digital image correlation

ABSTRACT

Metallic materials frequently undergo fatigue failure during long-term service. Therefore, the study of fatigue performance detection methods with high precision and wide application ranges is crucial to reduce fatigue failures and accidents of materials and structures. In this study, a plastic strain incremental energy dissipation theory (PSIEDT) is established, and a general expression for fatigue limit is derived with the starting point of the plastic strain increment. Taking 42CrMo4 steel as an example, and its temperature and deformation fields are obtained synchronously using infrared thermal imaging and digital image correlation. Its fatigue limit is evaluated using the energy dissipation theory based on the plastic strain increment. The results show that the relative error between the fatigue limit measurement accuracies of the developed method and the method proposed by Luong is 1.64 %. The relative error of the fatigue limit obtained for the local damage region is only 0.18 %, which has a high measurement accuracy. At the microscopic level, the onset of plastic strain corresponds to a change in the microstructure of the material from reversible deformation (viscoelastic) to permanent deformation (plasticity). Therefore, the strain measurements have higher sensitivity than the temperature measurements. Considering the limited heat release of many materials, the new method has a wide application range, can rapidly obtain material fatigue properties, and has good engineering application prospects.

1. Introduction

With the rapid development of the machinery industry in recent years, the application of various high-strength alloy steels has increasingly widened, particularly in transportation, aviation, aerospace, shipping, and pressure vessels. For example, among these materials, 42CrMo4 steel has good comprehensive properties, such as high strength, toughness, and good hardenability. With modulation, it exhibits good toughness and fatigue resistance, and it is commonly used in the manufacture of mechanical components (such

* Corresponding author.
E-mail address: liuzw@bit.edu.cn (Z. Liu).

https://doi.org/10.1016/j.engfracmech.2023.109173
Received 8 November 2022; Received in revised form 28 February 2023; Accepted 1 March 2023
Available online 5 March 2023

Table 1
Comparison of current main infrared thermal imaging methods.

Method	Fatigue limit definition	Method principle	Advantage	Disadvantage
Risitano method [28–30]	Minimum stress causes the surface temperature to rise.	One-line method: (σ_e is the fatigue limit, σ_a is the stress level of the experimental loading at all levels) $\begin{cases} \Delta T_{AS} = 0 & (\sigma_a \leqslant \sigma_e) \\ \Delta T_{AS} = A\sigma_a + B & (\sigma_a > \sigma_e) \end{cases}$	Data processing is relatively simple.	Phenomenological theory, predictions are often too conservative.
Luong method [18,31,32]	Minimum stress that produces inherent dissipation.	Two-line method: $\begin{cases} \Delta T_{AS} = A\sigma_a + B & (\sigma_a \leqslant \sigma_e) \\ \Delta T_{AS} = C\sigma_a + D & (\sigma_a > \sigma_e) \end{cases}$	Various heat sources are analyzed using thermomechanical coupling equations, and it is proposed to use inherent dissipation sources as fatigue damage parameters.	It is difficult to determine the critical cyclic stress amplitude directly related to the intrinsic dissipation of the material.
Crupi method [20–24]	Minimum stress to generate internal friction.	Quadratic function method: $\begin{cases} \Delta T_{AS} = 0 & (\sigma_a \leqslant \sigma_e) \\ \Delta T_{AS} = A\sigma_a^2 + B & (\sigma_a > \sigma_e) \end{cases}$	Link fatigue damage to internal friction theory.	There are few experimental proofs, which are not enough to explain the accuracy of the prediction results of this method.
Lock-in thermal imaging [25]	Minimum stress causes thermoelastic temperature drift.	Thermo-mechanical coupling equation: $\rho_0 C_T \dot{\theta} - k\nabla_0^2\theta = \rho_0 h + w'_{ctm} + w'_c$ (θ is the absolute temperature, $\rho_0 h$ is the external heat source in the initial configuration, w'_{ctm} is the thermodynamic coupling effect, w'_c is the energy dissipation density)	The drift value of the measured temperature rise caused by thermoelasticity relative to its theoretical value is used as the fatigue evaluation index.	The D mode of the JADE phase-locked infrared thermal imaging system produced by the French CEDIP company needs to be enabled to separate and extract the temperature rise ΔT_d corresponding to the energy dissipation term w'_c in the thermal–mechanical coupling theory.

as gears) [1,2]. The main failure form of an engineering structure is fatigue fracture, accounting for 50–90 % of mechanical failures. Many major accidents such as bridge fractures, house collapses, traffic accidents, and plane crashes are related to metal fatigue fractures [3–5]. In the actual service process of materials, most mechanical failures are caused by metal fatigue, causing significant economic losses. Mechanical components mostly undergo fatigue failure during long-term service. Fatigue damage is an important factor affecting the service life of a mechanical component. Therefore, it is of great significance to study the fatigue mechanism and fatigue performance testing methods of metal materials for reducing the fatigue failure and accidents of components [6].

Owing to the many factors affecting the fatigue properties of metals, accurate prediction of the fatigue properties of metallic structures is difficult. The traditional methods to obtain the fatigue limit mainly include single-point method [7], group method [8], lifting method [9] and other methods [10]. Obtaining the fatigue performance of materials based on mathematical statistics frequently requires many samples and is time-consuming [11]. For example, typically, more than 15 samples and 15 days are needed to predict fatigue strength by the lifting method. However, in engineering practice, more than 15 experiments are frequently required to improve the confidence level. As an emerging fatigue research method, fatigue thermal imaging [12,13] is based on the energy dissipation theory and infrared thermal imaging technology. It records thermal imaging data of the surface of a specimen under cyclic loading and analyses as well as estimates the fatigue properties of the produced material or component in combination with relevant theories. Fatigue thermal imaging has many advantages, such as few samples and non-contact, fast, non-destructive, and real-time measurements. It has been used to rapidly determine the fatigue limit, fatigue life, and S—N curves of materials and components.

Risitano et al. [14] first proposed using thermal imaging to rapidly determine the fatigue limits of materials. They fitted the data points after an abrupt change in the temperature rise as a straight line and defined its intersection with the abscissa (stress) as the fatigue limit. The Luong method [15,16] uses an inherent dissipation source as the research object and linearly fits the data before and after the abrupt temperature increase point generated by its inherent dissipation. The intersection of the two lines is the fatigue limit. However, when Luong proposed this method, he did not specify how to collect the data; therefore, studies may obtain inconsistent results when using it. Considering this, Wang [17] proposed a new method based on the Luong method to address the problem of ambiguity in the inherent dissipation inflection points of some materials. In this method, discrete points before and after the inflection point in the temperature rise–stress diagram are fitted to two straight lines. The slopes are denoted as K_1 and $K2$, and the intersection of the two lines is considered the fatigue limit of the corresponding material when slope $K2$ of the second straight line reaches the maximum. From the perspective of the heat generation mechanism, according to Liu et al. [18,19], the inflection point is due to a change in the heat generation mechanism. Under the combined action of various heat generation mechanisms, the temperature of a material changes during the fatigue process. Specifically, when the stress loading is lower than the fatigue limit, the non-plastic effect dominates energy dissipation, causing a small temperature increase on the sample surface. By contrast, when the stress loading is higher than the fatigue limit, the non-plastic and plastic effects act together, causing a large temperature rise on the sample surface. However, when the stress loading is close to the fatigue limit, the mechanism that dominates the temperature change is complex, causing the temperature rise mechanism to vary. According to Crupi [20] and Audenino [21], fatigue damage is caused by internal friction. When subjected to cyclic stress, each part of a material moves relative to the other parts, generating internal friction. After processing a large amount of test data, Crupi et al. [22] determined that when the fatigue load stress exceeds the fatigue limit, the square of the load stress amplitude and the temperature rise are linearly related. When the fatigue load stress is below the fatigue limit, the temperature increase on the sample surface is very small, and it can be approximated that no temperature increase occurs. Crupi [23] and Canteli [24] used a single-line method model in infrared thermal imaging to predict the fatigue limits of welded structural samples. They observed defects, such as microcracks, inside the samples, which caused fatigue failure; however, their fatigue limit prediction results had low accuracy. Therefore, according to Crupi et al., infrared thermal imaging can only be applied to cases in which cracks start from the specimen surface. Bremond and Potet [25] proposed the lock-in thermal imaging method and developed a data-processing mode (D-MODE), which was consistent with the former. The basic principle of D-MODE is that fatigue failure is a process of continuous damage accumulation, 60 % of which is due to local damage. Kelvin's thermoelastic equation is used to quantify the temperature rise caused by thermoelasticity. This part of the temperature rise is subsequently deducted from the overall temperature rise using the phase-locking method, and only the inelastic energy in the fatigue process dissipation is studied. Krapez et al. [26,27] performed fatigue tests on various alloys using lock-in thermal imaging. Different from the Luong method [16], this method does not study the overall energy dissipation; it performs data processing instead. The drift of the measured temperature rise caused by thermoelasticity relative to its theoretical value is used as the fatigue evaluation index. Therefore, owing to the introduction of a thermomechanical coupling equation and the energy dissipation theory, the fatigue limit by the Luong method [16] has a clear physical relevance, and this method is currently the most commonly used. Based on Table 1, presently, the main methods for measuring fatigue limit by infrared thermal imaging and the corresponding advantages and disadvantages are as follows.

Although fatigue thermal imaging has achieved good results in detecting the fatigue limits of materials and components, different materials have different temperature rise–stress curves owing to their different thermophysical properties. For materials with insignificant energy dissipation and temperature changes that do not conform to a 'three-stage temperature rise', the mathematical model of infrared thermal imaging needs to be corrected according to the material characteristics to obtain accurate detection results.

Digital image correlation (DIC) is used to measure the three-dimensional coordinates, displacement, and strain of the object surface during deformation by tracking speckle images on the object surface, and is mainly applied to the measurement and acquisition of full-field strain, deformation, displacement, amplitude, mode and other information. Compared with other deformation measurement methods, DIC has the following advantages [33,34]. It can realise long-term observation in a complex environment, does not require complex processing of a sample, involves simple preparation, and has high universality. Samples of a wide range of sizes can be tested, from micrometers to tens of metres. Moreover, DIC can obtain the full-field deformation information on the sample surface, which is beneficial for the subsequent full-field strain analysis.

In recent years, DIC has been more and more applied in the field of fatigue research, and a large number of studies have been conducted in the strain field evolution [35–37], crack growth laws [38–40] and fatigue performance [41–43]. In the study of strain field evolution during fatigue, Zou et al. [35] used DIC to observe the strain field changes in traditional fatigue experiments and found that the fracture position of a specimen was consistent with the stress concentration position in the fatigue loading process. Based on DIC technology, a new method for shortening the traditional fatigue experiments was proposed. Favier et al. [36] used infrared thermal imaging and DIC technologies to observe a TiNi shape memory alloy in a tensile experiment and determined its deformation mechanism by analysing the evolution of the temperature and strain fields. In the study of fatigue crack growth laws, Gao et al. [38,39] studied the relationship between the strain amplitude of the crack tip and the number of fatigue cycles when a fatigue crack did not expand. The change laws of the displacement and strain fields in the crack tip region were obtained using the DIC method when the fatigue crack expanded to different lengths. Duan et al. [40] proposed a new parameter for evaluating fatigue crack closure—crack opening ratio (COR). By means of bi-prism-based single-lens 3D digital image correlation (BSL 3D DIC) technique, the full-field fatigue deformation near the crack tip was in situ measured, based onl which the crack opening load COL was characterized throughout the whole process of fatigue tests. The result was less dispersion and better noise immunity. In the study of fatigue performance, Chrysochoos et al. [41] evaluated the fatigue properties of materials by combining infrared thermal imaging and DIC technology. Duan et al. [42] proposed a new distortion calibration technique for bi-prism-based single-lens 3D digital image correlation (BSL 3D DIC) to in-situ and online characterize 3D full-field deformation with high precision, and anisotropic mechanical behavior of nickel-based single crystal superalloy (NBscs) was studied.

At present, with the rapid application of infrared thermal imaging technology in the fatigue field, some researchers have discussed the relationship between material heat dissipation and strain change during fatigue process. Zhou et al. [44] used an infrared thermal imager to record the temperature rise process of a sample and installed an extensometer on the sample to measure its strain during the experiment. The internal relationship between the heat dissipation and strain change law of the material under a gradient alternating load was preliminarily examined. Cao et al. [45] studied the strain and microstructure evolution during fatigue cyclic stress loading through DIC technology and positioning tracking observation experiments. The corresponding relationship between the microstructure evolution and the inherent dissipation mechanism transformation when a material experienced an elastic–plastic transformation was revealed. Liu et al. [46] evaluated the fatigue limit of a material from the accumulated strain and temperature dissipation values in the stable stage of fatigue deformation. However, they did not analyse the deformation of the material during cyclic loading and did not provide a detailed theory. Therefore, DIC technology can yield the full-field strain of a material, enabling effective analysis of its deformation during the fatigue process.

The paper takes 42CrMo4 steel as an example. From the perspective of the heat generation mechanism, a new plastic strain increment energy dissipation theory (PSIEDT) was established based on the energy dissipation theory and infrared thermal imaging. This method was used to obtain the fatigue limit, and it realised the equivalent acceleration of the experimental process. Using infrared thermal imaging and DIC technologies, a set of fatigue performance testing and observation systems were built, and the temperature and deformation of the sample surface were obtained synchronously by setting a fatigue loading programme. The feasibility of this method for obtaining the fatigue limit was verified by comparing its use with that of the Luong method [16] in fatigue thermal imaging. Combining the analyses of the evolution characteristics of the overall strain and strain fields in the local damaged region, the accuracy of the method was further verified. Based on the energy dissipation theory, the physical significance of this method was analysed from macro and micro perspectives to further prove its reliability. The fatigue properties of the material were rapidly acquired, detection accuracy was improved, and engineering application of this method was promoted.

2. Methodology

2.1. Energy evolution during deformation

Under the action of alternating loads in fatigue experiments, a specimen deforms, and its deformation includes elastic and inelastic deformations. The deformation process of a sample is accompanied by energy dissipation, and energy transformation occurs inside the material. The mechanical work (mechanical energy consumption) performed by the applied load on the material is converted into elastic strain energy by the elastic deformation inside the material and into viscoelastic and plastic strain energies by the inelastic effect [47]. Elastic strain energy is the reversible deformation energy of the internal lattice when the material is elastically deformed, which does not affect the fatigue damage. Most of the viscoelastic strain energy is stored inside the material, whereas the remainder is dissipated into the environment as energy. Plastic strain energy is the main cause of cumulative damage to the material. It is stored in the microscopic defects inside the material, and most of it is dissipated in the form of heat [48]. The remaining small part is lost in other forms, such as acoustic emission, and is ignored.

During the fatigue experiment, according to the first law of thermodynamics and the law of conservation of energy, the mechanical work W consumed by a unit volume of material in a cycle is converted into heat Q and internal energy U. Finally, the relationship is expressed as follows [49]:

$$W = Q + U \tag{1}$$

According to the stress σ-strain ε curve in the tensile process, the mechanical work W done by the external force can be expressed as follows:

$$W = \oint f(\sigma) \cdot \mathrm{d}\varepsilon \tag{2}$$

The change in internal energy U during the deformation process is mainly composed of the internal energy change U_1 caused by the material temperature rise and the material damage amount U_2 in the deformation process, which can be expressed as follows [47]:

$$U = U_1 + U_2 = \frac{1}{f}(\rho_0 \cdot C_T \cdot \frac{\partial T}{\partial t}) \cdot V + U_2 \tag{3}$$

Among them, ρ_0 is the material density, C_T is the constant pressure specific heat, and T is the temperature field associated with t, f is frequency and t is time, V is the material volume.

The heat Q under the applied load mainly includes three parts [50]: heat conduction, heat convection and heat radiation. Correspond to the first, second, and third terms on the right side of Eq. (4), respectively, as follows:

$$Q = \frac{1}{f}(\int A_{cd}\lambda \cdot gradT \cdot \overrightarrow{n} \cdot \mathrm{d}A_{cd} + \int A_{cv}\alpha_c \cdot (T - T_0) \cdot \mathrm{d}A_{cv} + \int A_{ir} e \cdot \beta \cdot (T^4 - T_0^4) \cdot \mathrm{d}A_{ir}) \tag{4}$$

In Eq. (4), λ is the thermal conductivity, α_c is the thermal convection coefficient, T is the specimen surface temperature, T_0 is the ambient temperature, e is the radiation coefficient, β is the Boltzmann constant,A_{cd}, A_{cv} and A_{ir} are heat conduction, heat convection, and heat radiation area, respectively. Among them, the heat conduction of the material during the deformation process makes the temperature uniform, the heat convection makes the energy exchange between the sample and the environment, and the heat radiation is the spontaneous process of the material. The heat radiation is the important information captured by infrared thermal imaging.

In conclusion, Eq. (1) can be expressed as follows:

$$\left(\oint f(\sigma)\mathrm{d}\varepsilon\right)V = \frac{1}{f}\left(\int A_{cd}\lambda gradT\overrightarrow{n}\mathrm{d}A_{cd} + \int A_{cv}\alpha(T - T_0)\mathrm{d}A_{cv} + \int A_{ir}e\beta(T^4 - T_0^4)\mathrm{d}A_{ir}\right) + \frac{1}{f}\left(\rho_0 C_T\frac{\partial T}{\partial t}\right)V + U_2 \tag{5}$$

According to Eq. (5), it can be known that stress and plastic deformation are important factors affecting energy dissipation. With the increase of stress and deformation, the internal energy and heat dissipation of the material will increase. Therefore, the temperature effect on the surface of the sample is the result of the dynamic balance between the heat generation and heat dissipation of the material under the action of external force in the deformation process.

2.1.1. Energy evolution during elastic deformation

The thermoelastic effect refers to the phenomenon that in elastic deformation, ferroelastic materials will release or absorb heat when they are elongated or shortened, and the entropy change is related to the deformation amount. Thermoelastic effects relate temperature to stress and elastic strain and lead to temperature oscillations with each fatigue cycle. In isotropic elastomers, the relationship between thermal stress and strain is as follows [51]:

$$\Delta\varepsilon_e = \frac{(1 - 2\nu) \cdot \Delta\sigma_e}{E} + 3\alpha\Delta T \tag{6}$$

where $\Delta\varepsilon_e$ is the elastic strain, $\Delta\sigma_e$ is the change in elastic stress, E is the elastic modulus, ν is the Poisson's ratio, α is the coefficient of linear expansion, and ΔT is the temperature change caused by the thermoelastic effect.

The following expression can be derived from the dynamic analysis of elastomer under reversible and adiabatic conditions [52]:

$$\Delta T = -3 \cdot \frac{T\alpha K\Delta\varepsilon_e}{\rho_0 C_V} \tag{7}$$

Where T is the absolute temperature, C_V is the isothermal specific heat and K is the bulk modulus.

By combining Eq. (6) and Eq. (7) through the conversion relationship between C_V andC_T, the equation is as follows [52]:

$$\Delta T = T - T_0 = -\frac{\alpha}{\rho_0 C_T} \cdot T \cdot (\sigma_1 + \sigma_2 + \sigma_3) \tag{8}$$

In Eq. (8), T_0 is the room temperature, $\sigma_i (i = 1, 2, 3)$ is the principal stress. If the absolute temperature of the specimen does not change much during each fatigue cycle, the temperature will be proportional to the first principal invariant of stress. Therefore, this equation can be used to analyze the thermoelastic effect of solid materials under adiabatic conditions.

2.1.2. Energy evolution during inelastic deformation

(1) Viscoelastic deformation behavior.

When the loading stress is lower than the fatigue limit and higher than the cyclic elastic limit, a viscoelastic material experiences a

viscous effect due to the phase difference between the strain and the stress. This effect causes the viscoelastic material to show a small temperature rise in an early fatigue test. This effect is called the viscoelastic effect and is described well by the Voigt–Kelvin model. The Voigt–Kelvin model consists of two parts that describe the elastic and viscous behaviour of the material respectively. Its expression is as follows [19]:

$$\sigma = \sigma_1 + \sigma_2 = E\varepsilon + J\dot{\varepsilon} \tag{9}$$

Among them, E and J are the elastic coefficient and viscosity coefficient, ε and $\dot{\varepsilon}$ are the strain and strain rate. Setting the sample loading load to$\sigma(t) = \sigma_0 e^{i\omega t}$, the relationship between the experimental duration and the sample strain is as follows:

$$\varepsilon(t) = A_1\sigma(t) - \frac{A_2\dot{\sigma}(t)}{\omega} \tag{10}$$

In the Eq.(10), A_1 and A_2 are parameters related to the viscosity of the material at each stress level, ω is angular frequency.

In the early stage of the fatigue experiment, due to the stress effect of cyclic loading, the mechanical work W per unit volume of material per cycle can be determined from the stress–strain curve, as shown in Eq.(11):

$$W = \oint \sigma \mathrm{d}\varepsilon = [A_1\frac{\sigma^2(t)}{2}]_0^T - \frac{A_2}{\omega}\oint \sigma \mathrm{d}\dot{\sigma} \tag{11}$$

Let$\sigma(t) = \sigma_0\cos\omega t$, then:

$$W_d = -\frac{A_2}{\omega}\oint \sigma \mathrm{d}\dot{\sigma} = \omega A_2\sigma_0^2\int_0^T \sigma(t)\mathrm{d}t = \frac{\omega A_2\sigma_0^2 T}{2} \tag{12}$$

According to Eq.(12), the average energy consumption D of materials per unit time is as follows:

$$D = \frac{1}{2}\sigma_0^2\omega A_2 = \pi f\sigma_0^2 A_2 \tag{13}$$

Therefore, combined with Eq. (9)–(13), the energy consumption of the material under the alternating load under the Voigt-Kelvin model is as follows:

$$D = \frac{\sigma_0^2}{2}\frac{J\omega^2}{E^2 + J^2\omega^2} = \frac{2\pi^2 Jf^2\sigma_0^2}{E^2 + 4\pi^2 J^2 f^2} \tag{14}$$

Therefore, under the action of low load, the relative energy consumption of the specimen can be expressed according to the Voigt-Kelvin model when hysteretic deformation occurs.

(2) Plastic deformation behavior.

The viscoelastic effect is caused when the load is low. When the loading stress is higher than the fatigue limit, owing to the relative shear movement in the crystal and the intergranular plastic deformation during dislocation slip, the crystal experiences internal friction. Therefore, the atoms oscillate, generating heat, which causes irreversible damage to the material. Moreover, the internal energy of the specimen sharply increases, and its surface temperature increases.

The heat Q generated by the material during deformation can be expressed as follows [53]:

$$Q = \rho_0 C_T\frac{\partial T}{\partial t} \tag{15}$$

Under cyclic stress, plastic accumulation occurs in the sample. The energy that specimen absorbed during plastic deformation can be obtained from the area enclosed by the cyclic stress–strain curve, which is also called the hysteresis loop. Therefore, the plastic deformation energy W_i of the specimen under cyclic strain is as follows:

$$W_i = \int_{\varepsilon_0}^{\varepsilon_1}\sigma_{\max}\mathrm{d}\varepsilon - \int_{\varepsilon_0}^{\varepsilon_1}\sigma_{\min}\mathrm{d}\varepsilon = A_i \tag{16}$$

Among them, ε_0 , ε_1 represent the minimum and maximum strain during a cycle,$\sigma_{\min}$, $\sigma_{\max}$ represent the minimum and maximum stress during the cycle, W_i represent the absorbed energy under the "i" cycle, and A_i is the stress–strain hysteresis loop area.

However, the energy in the deformation process is not all converted into heat, so the heat conversion rate η is introduced, it can be obtained as follows [54,55]:

$$\rho_0 C_T\Delta T_i = \eta\cdot\int_{\varepsilon_0}^{\varepsilon_1}(\sigma_{\max} - \sigma_{\min})\mathrm{d}\varepsilon \tag{17}$$

Therefore, the quantitative relationship between the temperature field ΔT_i and the stress–strain field (σ - ε) in the plastic deformation process is as follows:

$$\Delta T_i = \frac{\eta}{\rho_0 C_T}(\int_{\varepsilon_0}^{\varepsilon_1}\sigma_{\max}\mathrm{d}\varepsilon - \int_{\varepsilon_0}^{\varepsilon_1}\sigma_{\min}\mathrm{d}\varepsilon) \tag{18}$$

Therefore, under the condition of fatigue loading, the temperature change of the material surface has a great relationship with the stress, and the stress is the key factor determining the energy consumption of the material.

2.2. Plastic strain incremental energy dissipation theory

2.2.1. Energy dissipation theory

Under the framework of related thermodynamics theory mentioned in the previous section, to describe the irreversible thermodynamic process in the fatigue damage process, Chrysochoos [56] constructed the local thermomechanical coupling equation (Eq. (19)) during the fatigue loading process based on the energy balance theory. The left side of the equation represents the heat stored by the material through temperature changes, while the right side of the equation represents the four heat sources that cause the temperature change on the surface of the sample: an external heat source (r_{ext}), heat transfer source ($\lambda\ \Delta T$), thermoelasticity source (S_{th}), and inherent dissipation source (d_1).

$$\rho_0 C_T \frac{\partial T}{\partial t} = r_{ext} + \lambda \Delta T + S_{th} + d_1 \tag{19}$$

To simplify the local thermo-mechanical coupling equations, assumptions are as follows: (1) The thermal conductivity remains constant during the experiment and the thermal conductivity of the material is anisotropic; (2) Material density and specific heat are material constants; (3) The external heat source r is a constant that does not change with time. Since the temperature caused by thermoelasticity changes periodically and the energy accumulation is 0 in a complete cycle, Eq. (19) can be simplified as follows:

$$\rho_0 C_T \frac{\partial T}{\partial t} = d_1 \tag{20}$$

Thus, the relationship between the temperature change and the inherent dissipation during the fatigue process is clarified, showing that the inherent dissipation is the main heat source of the temperature change of the sample surface. According to Section 2.1, in the fatigue process of metallic materials, the inherent dissipation mainly originates from two parts [57]: one part is non-damaging effects such as viscoelasticity, and the other is plastic effects. When the cyclic stress level is lower than the fatigue limit, the inherent dissipation of a metallic material is only caused by viscoelasticity and its internal structural change is reversible; thus, no substantial damage is caused. When the cyclic stress level is higher than the fatigue limit, owing to irreversible movements, such as dislocation movements, multiplication, delivery, accumulation, and microplastic deformation begins to appear. Moreover, the inherent dissipation is dominated by the microplastic effect, and the material begins to exhibit fatigue damage and accumulation continuously. Therefore, according to the energy dissipation theory, the Luong method [16] linearly fits the data before and after the abrupt change in the temperature rise caused by the inherent dissipation, and the intersection of the two lines is the fatigue limit.

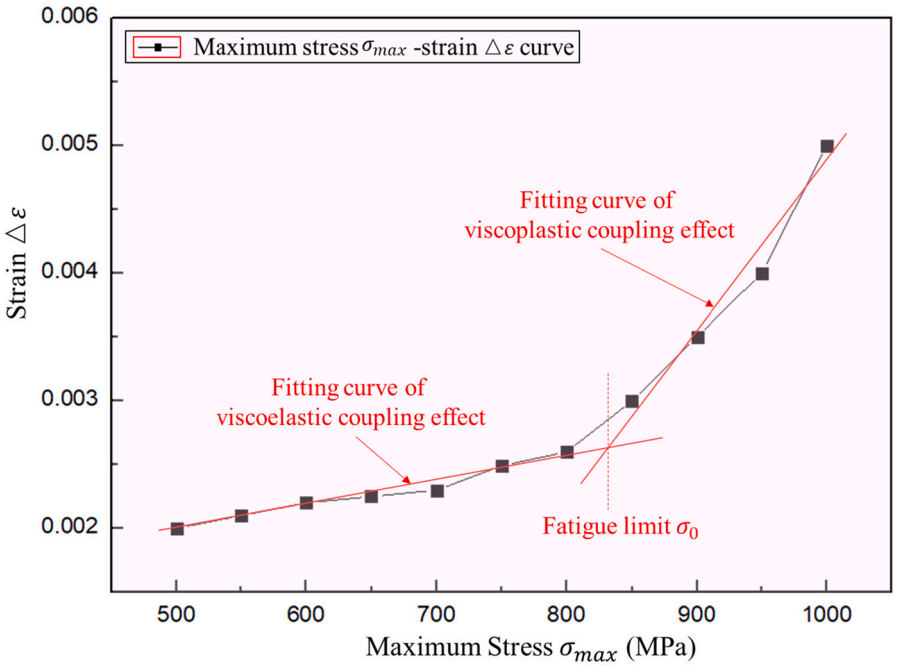

Fig. 1. Schematic diagram of the relationship between stress and strain under different stress amplitudes.

2.2.2. Plastic strain incremental energy dissipation theory

Through the theoretical analysis presented above, plastic deformation is the fundamental cause of the increase in the sample surface temperature. Therefore, the heat generation of the sample is directly related to its deformation. The work done by a testing machine on the sample directly affects its strain in the fatigue experiment process, and owing to the change of strain, the state and number of dislocations, slips, lattice distortions, etc. inside the sample change, leading to the increase of sample temperature. However, in practical engineering applications, the temperatures of some parts cannot be measured directly. Therefore, combined with the strain change law during the experiment process, infrared thermal imaging was used as an aid, and the plastic strain increment was used as a characteristic parameter to rapidly predict the fatigue limit. The PSIEDT is described as follows.

It can be seen from Subsection 2.1 that the heat generation mechanism of fatigue mainly has two parts: viscous part and plastic part. Therefore, the linear law of strain caused by load under the fatigue limit is inconsistent with that caused by load above the fatigue limit. It is possible to fit the lines with different slopes, since the mechanism that generates the energy dissipation always turns around the fatigue limit. To distinguish different heat generation mechanisms, the assumptions are as follows:

(1) It is assumed that the constitutive relationship of the material is bilinear. That is to say, the strain caused by the load below the fatigue limit and the strain caused by the load above the fatigue limit are approximately linear;
(2) Material viscosity is a property of the material itself and is independent of the loading state. It is assumed that the strain caused by the viscous effect below the fatigue limit and above the fatigue limit is approximately in the same straight line as the loading level.

Based on the above assumptions, the slope below the fatigue limit is defined as k_1 and the slope above the fatigue limit is defined as k_2. The relative energy consumption of the sample under the action of low load can be expressed according to the Voigt-Kelvin model. The constitutive equation is shown in Eq. (9). Fig. 1 shows the relationship between stress σ and strain $\Delta\varepsilon$ under different stress amplitudes, and the linear equation under low load is expressed as follows:

$$\Delta\varepsilon = k_1 \cdot \sigma - b_1 \tag{21}$$

where k_1 and b_1 are linear fitting coefficients.
Substitute Eq. (9) into Eq. (21), as follows:

$$\Delta\varepsilon = k_1 \cdot (E\varepsilon + J\dot{\varepsilon}) - b_1 \tag{22}$$

Rewrite it as follows:

$$\Delta\varepsilon + b_1 = k_1 \cdot E\varepsilon + k_1 \cdot J\dot{\varepsilon} \tag{23}$$

In Eq. (23), the first term on the right side of the equation is the elastic term, and the second term is the viscous term. k_1 is the slope of the straight line, E and J are the elastic and viscous coefficients, and ε and $\dot{\varepsilon}$ represent the strain and strain rate. Since the average temperature rise caused by the thermoelastic effect is 0, the first term on the right side of Equation (23) is 0, Eq. (23) can be rewritten as follows:

$$\Delta\varepsilon + b_1 = k_1 \cdot J\dot{\varepsilon} \tag{24}$$

Among them, the strain rate $\dot{\varepsilon}$ represents the strain amount of the material per unit of time. Considering that under the action of fatigue load, the average strain rate of one cycle can be approximately equal to the product of the strain amount ε in each cycle and the loading frequencyf_z, as follows:

$$\Delta\varepsilon + b_1 = k_1 \cdot J\dot{\varepsilon} = k_1 \cdot J \cdot \varepsilon \cdot f_z \tag{25}$$

Rewrite it as follows:

$$\Delta\varepsilon = \frac{k_1 f_z}{E} J \cdot \sigma - b_1 \tag{26}$$

The above equation is the relationship between the viscous effect and the strain of the material, and the viscosity coefficient J can be obtained according to the relationship between the stress and the strain obtained by the fatigue test:

$$J = \frac{\Delta\varepsilon + b_1}{k_1 \cdot (\sigma/E) \cdot f_z} \tag{27}$$

According to assumptions (2), the strain caused by the viscous effect below the fatigue limit and above the fatigue limit is approximately in the same straight line as the loading level. Then the viscous part is removed from the heat generation mechanism above the fatigue limit is the plastic effect part. Thus, the viscous effect and the plastic effect in the viscoplastic coupling effect are separated. Therefore, the strain above the fatigue limit in Fig. 1 comes from the viscoplastic coupling effect, and the curve with the heat-generating mechanism of the viscoplastic coupling effect is approximately linearly fitted as follows:

$$\Delta\varepsilon = k_2 \cdot \sigma - b_2 \tag{28}$$

where k_2 and b_2 are linear fitting coefficients. Remove the viscous part from Eq. (28), and subtract Eq. (26), as follows:

$$\Delta\varepsilon = (k_2 - \frac{k_1 f_z}{E} J) \cdot \sigma - C \tag{29}$$

Eq. (29) expresses the relationship between the plastic effect and strain in the fatigue process, where C is a constant term. Thus, $\Delta\varepsilon = 0$, and the obtained stress value,σ_0, is the fatigue limit. As mentioned earlier, plastic deformation during material fatigue causes fatigue damage, and a viscous effect can change the strain or temperature rise; however, it does not lead to fatigue damage. Therefore, according to the energy dissipation theory, the fatigue limit of a material can be obtained using the starting point of the plastic strain increment as given in Eq. (29). Fig. 2 shows a flowchart of plastic strain incremental energy dissipation theory.

3. Experiment setup

In this section, a fatigue performance test and observation system was built, using which the temperature change process and surface deformation of the 42CrMo4 steel during the fatigue process were studied. A combined experiment using infrared thermal imaging and DIC was conducted. The applicability and reliability of the method were verified by comparing the results obtained by the PSIEDT with those by the Luong method [16].

3.1. Experimental materials

The material used in the experiment is 42CrMo4 steel. The material was processed into a standard plate fatigue specimen. The thickness t is 3 mm, as shown in Fig. 3. The sample should avoid overheating and work hardening during processing, and be ensured that the surface is smooth and clean. The surface of the sample should be polished without scratches and damage, so as not to affect the fatigue test.

3.2. Experimental method

(1) Experiment preparation

Before the experiment starting, it was necessary to spray speckles on the strain collection surface of the sample and calculate the correlation coefficient of the speckle image. When the overall correlation coefficient of the speckle image was greater than 0.98, the produced speckle was considered reliable. In addition, to ensure accurate temperature collection, the experiment should be carried out in a closed room with no air disturbance and no direct sunlight and the indoor temperature should be kept constant.

(2) Establishment of experimental system

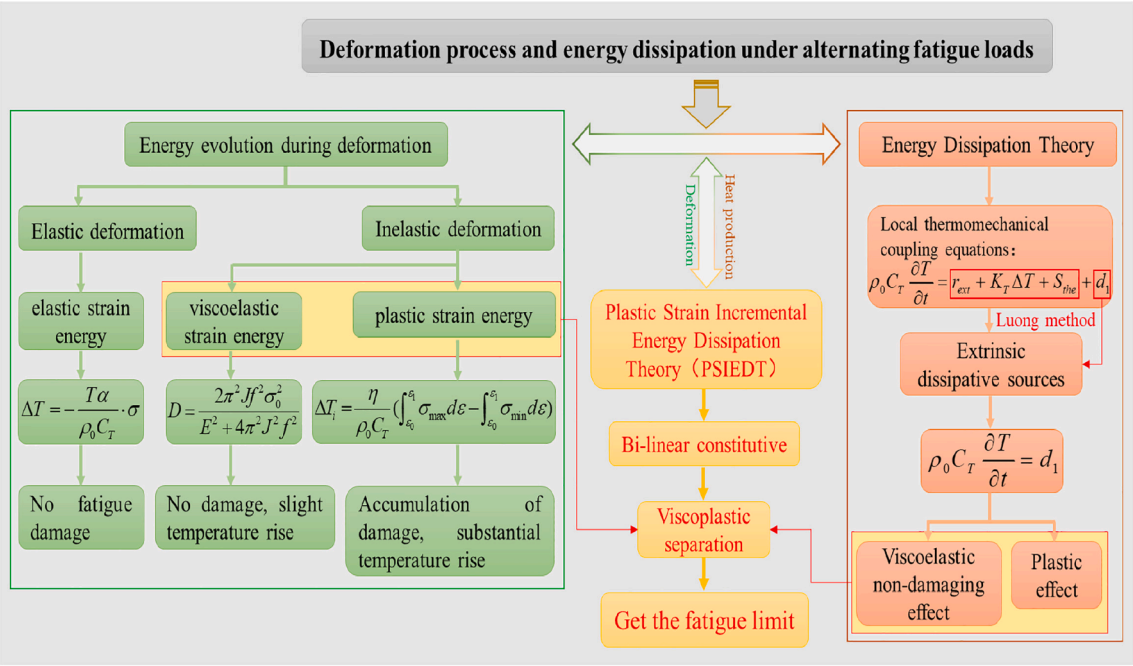

Fig. 2. Flowchart of plastic strain incremental energy dissipation theory.

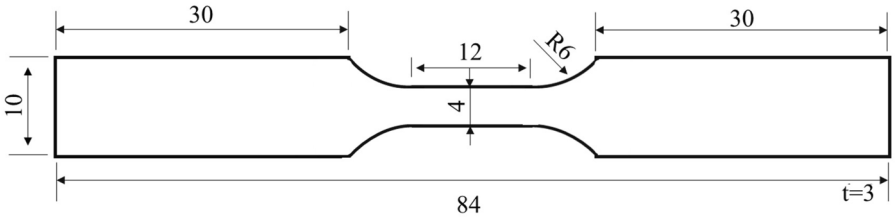

Fig. 3. Schematic diagram of fatigue specimen size (unit: mm).

The fatigue performance test and observation system is shown in Fig. 4, which consists of a MTS810 servo-hydraulic testing machine, an image acquisition system including the infrared experiment system (Infrared camera model: VariaCAM, resolution: 640 pixels × 480 pixels), DIC experimental system (Including microscope head and CMOS camera, among which CMOS camera model: mER-301-125U3M/C, resolution: 2048 pixels × 2048 pixels, exposure time: 20 μs–1 s), computer control system, etc. The infrared thermal imaging system is used to monitor and record the surface temperature of the sample and ambient temperature in real-time, and the DIC experimental system records the deformation of the sample surface, which is used to study the fatigue performance of the material.

(3) Image acquisition

After the device was connected, the focal length of the camera was adjusted such that the sample image in the acquisition software interface remained clear. During the fatigue experiment, the waveform was set as a sine wave, the stress ratio was 0.1, the loading frequency was 40 Hz, and the acquisition frequencies of the infrared and CMOS cameras were 50 Hz. Before the start of an experiment, original temperature and speckle maps were collected, and initial deformation image of the sample under different stress loadings were collected before the start of each experiment. At the beginning of a fatigue experiment, images of the temperature change of the specimen surface and deformation during loading were acquired synchronously.

In each experiment, loading was applied by increasing the cyclic stress step-wise. The maximum loading stress, σ_{max}, started at 200 MPa and ended when the yield limit was exceeded or the sample broke. The stress cycle of each stage was stopped when the surface temperature of the sample reached a stable state. After the previous stress level was loaded and the heat was fully dissipated, the stress level was increased to continue the experiment. Notably, the interval between the two experiments needed to be sufficiently long to ensure the surface temperature of the sample was consistent with the ambient temperature (generally about 10–15 min). The loading process is shown in Fig. 5. Before each experiment, the non-uniformity correction of the infrared camera was required to ensure the accuracy of the temperature measurement of the equipment. During the fatigue experiment, when the infrared camera was used to synchronously collect the temperature change of the surface of the sample, the real-time temperature value was recorded as T_s, and the ambient temperature was recorded as T_a, then the surface temperature rise of the sample was $\triangle T_{s0} = T_s\text{-}T_a$, and the temperature rise

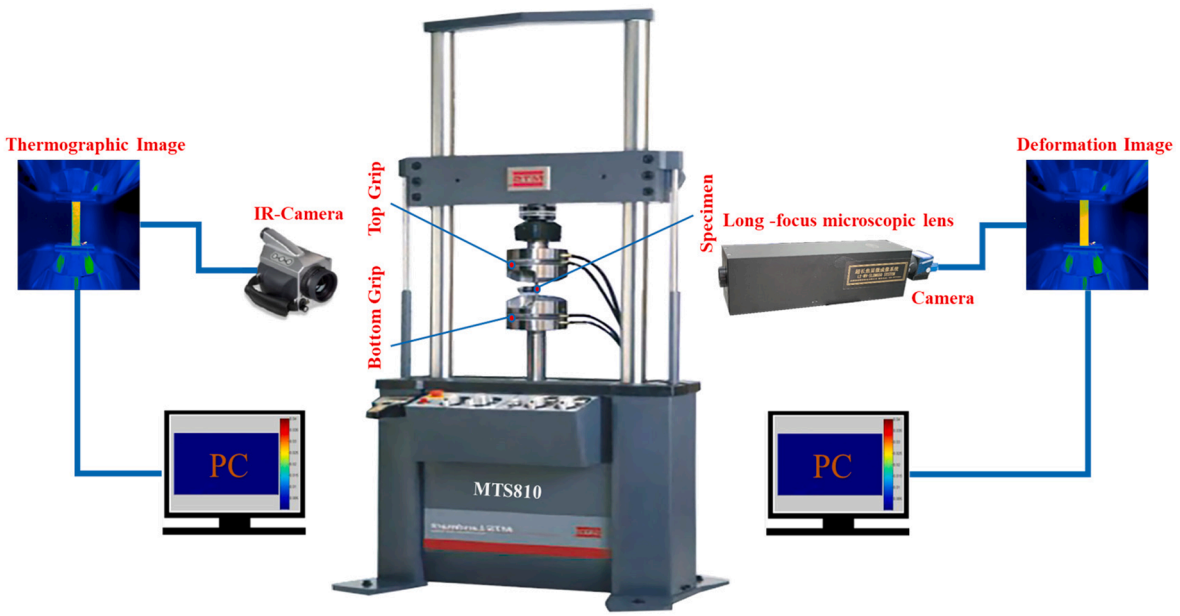

Fig. 4. Fatigue performance testing and observation system.

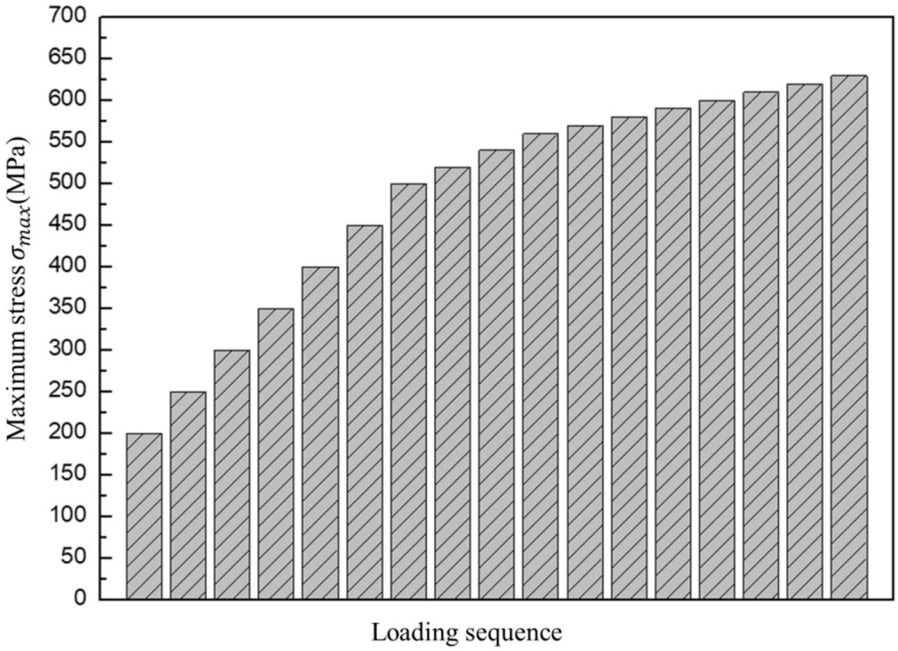

Fig. 5. Stress loading procedure.

value in the temperature stabilization stage was recorded as ΔT_s. The specific fatigue experimental parameters are shown in Table 2.

4. Experimental results and analysis

4.1. Fatigue limit obtained by infrared thermal imaging

By the step-wise loading experiments on a 42CrMo4 steel fatigue specimen, fatigue infrared thermal images under different loads were obtained. Fig. 6 shows the initial thermal image under no stress and the thermal image at 600 MPa. Because the variation in the temperature of the sample is small during the loading process, the steady-state temperature rise, $\triangle T_s$, after the cyclic loading at each stress level was used as the characteristic parameter to draw the temperature rise curves under different stress loadings. The result is shown in Fig. 7. When calculating the steady-state temperature rise $\triangle T_s$, as shown in the blue box in Fig. 6, it is calculated by selecting the entire working section of the sample as the region of interest for temperature averaging, and then subtracting the initial temperature. From the curves of the temperature rise under the different stress loadings (Fig. 7), it can be seen that all data points present two linear distribution trends with different slopes. Using the double-line fitting by Luong method [16], yielding the stress at the intersection point, i.e., the fatigue limitσ_0, as 568.06 MPa.

4.2. Research on fatigue limit obtaining method based on plastic strain incremental energy dissipation theory

4.2.1. Experimental data processing

As shown in Fig. 8(a), speckle images under different stresses were collected using the CMOS camera. The sample image before each stress loading was selected as the reference image (image in red box in Fig. 8(a)). The image after each stress loading is used as the deformation image to calculate the deformation field (image in blue box in Fig. 8(a)). To compare with the prediction results of the

Table 2
42CrMo4 fatigue experiment parameters.

Specimen ID	HR100206
Loading waveform	Sinusoidal wave
Stress ratio	0.1
Loading frequency	40 Hz
Loading stress value of each stage (MPa)	200/250/300/350/400/450/500/520/ 540/560/570/580/590/600/610/620/630
The determination of $\triangle T_s$	The average temperature rise at loading for a given number of cycles.
The number of load cycles at a given level	20,000 cycles
Stopping criterion	Total separation of fracture surfaces
Origin of fatigue fracture	Edge of the flat specimen

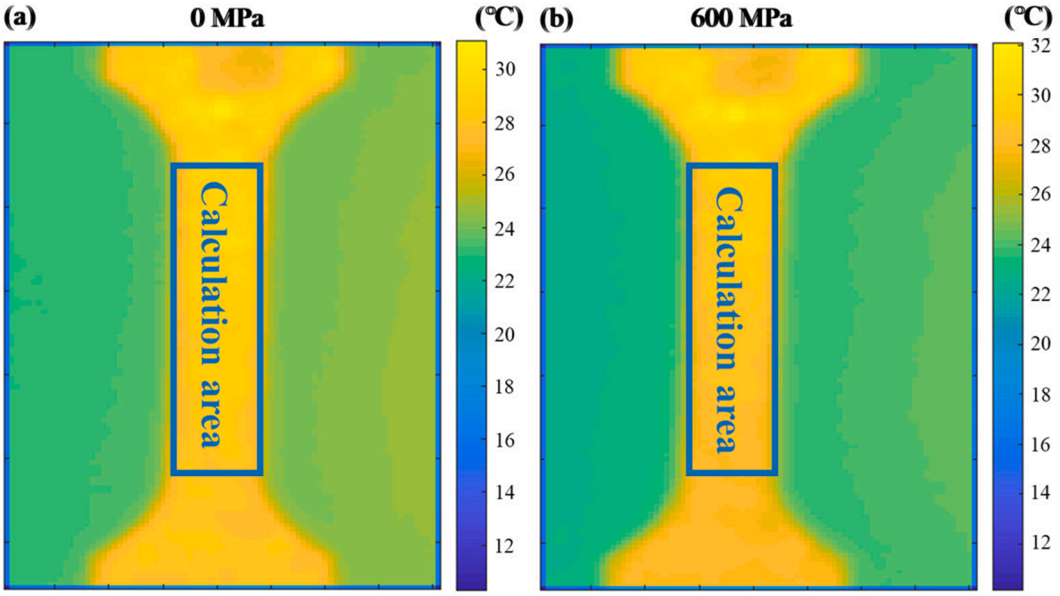

Fig. 6. Infrared thermal images under different stress loadings. ((a) Initial thermal image under no stress, (b) Thermal image at 600 MPa).

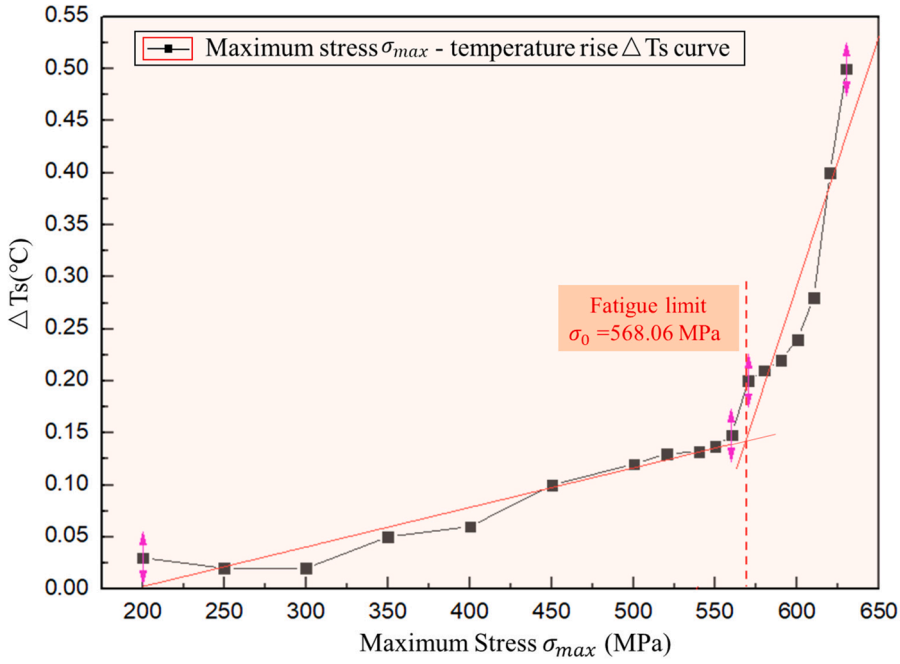

Fig. 7. Fatigue limit of 42CrMo4 steel sample obtained by the Luong method.

fatigue limit by the Luong method, the DIC calculation region should be consistent with that in Fig. 6. As shown in the green box in Fig. 8(a). During the calculation, the subregion size was 29 × 29 pixels, and the step size was 5 pixels, using the open source DIC code Ncorr of MATLAB (displacement resolution: 0.05 pixels, strain resolution > 100με) [58]. Subsequently, the average strains on the sample surface after the different stress loadings were calculated and the deformation values after different stress loadings were obtained, thereby yielding the deformation conditions of the sample after the different stress loadings. Fig. 8(b) shows the axial strain distributions on the sample surface after the different stress loadings. Noticeably, when the stress level is low, the induced strain is very small, and as the loading stress increases, the strain also increases.

The average strain of the selected region of the sample surface after a stress loading was selected, and the deformation size after the loading was calculated. Accordingly, the deformation conditions after the different stress loadings were obtained, and the results are

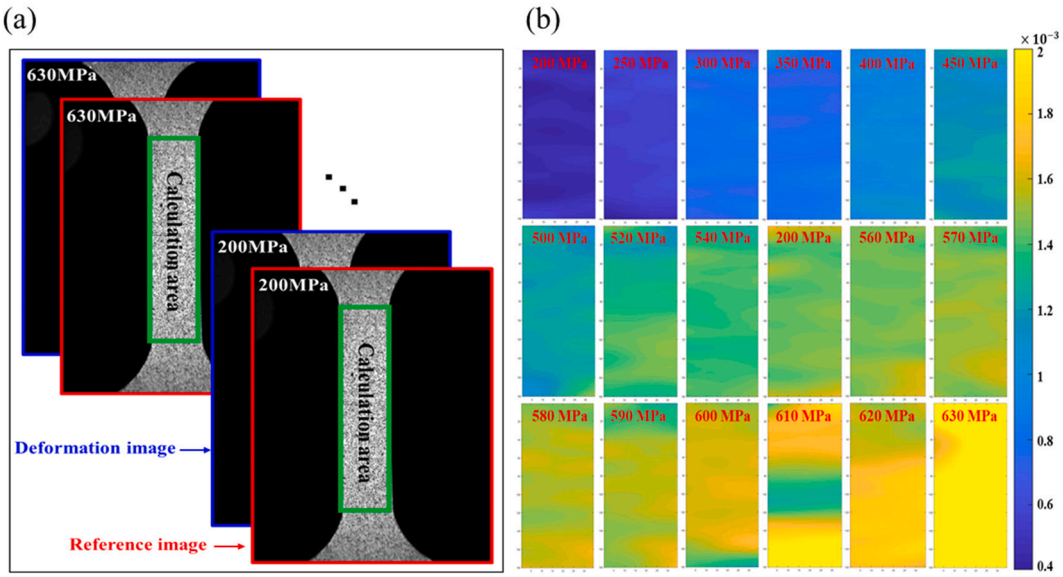

Fig. 8. Strain distribution of 42CrMo4 steel specimen under different stress loadings. ((a) Speckle images under different stress loadings, (b) Axial strain distribution on the specimen surface after with different stress loadings).

shown in Fig. 9. It can be observed that when the stress level is low, the amount of deformation is small, and as the stress gradually increases, the deformation increases, and permanent deformation begins to appear until the specimen breaks.

4.2.2. Fatigue limit obtained by PSIEDT method

Firstly, the elastic modulus E was calculated to be 204 GPa based on the experimental data. Secondly, for the average strain of the specimen surface under different stress loading, the method based on the plastic strain incremental energy dissipation theory proposed in Section 2.2.2 is used to obtain the fatigue limit. As shown in Fig. 10, the relationship between strain and stress under low load is fitted firstly, and the linear equation is expressed as follows:

$$\Delta\varepsilon = (4.7924 \times 10^{-6})\sigma + 3.8567 \times 10^{-5} \tag{30}$$

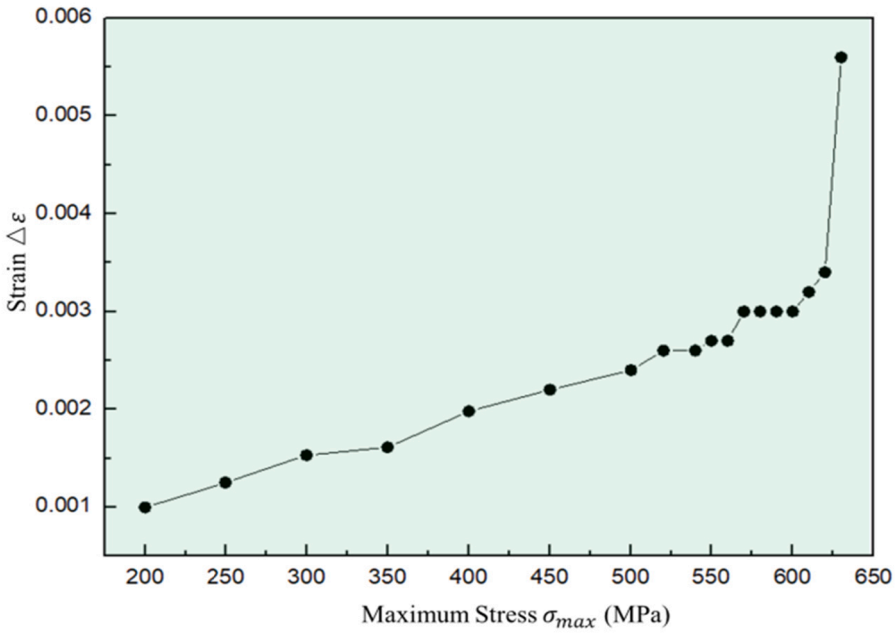

Fig. 9. The average strain on the specimen surface under different stress loadings.

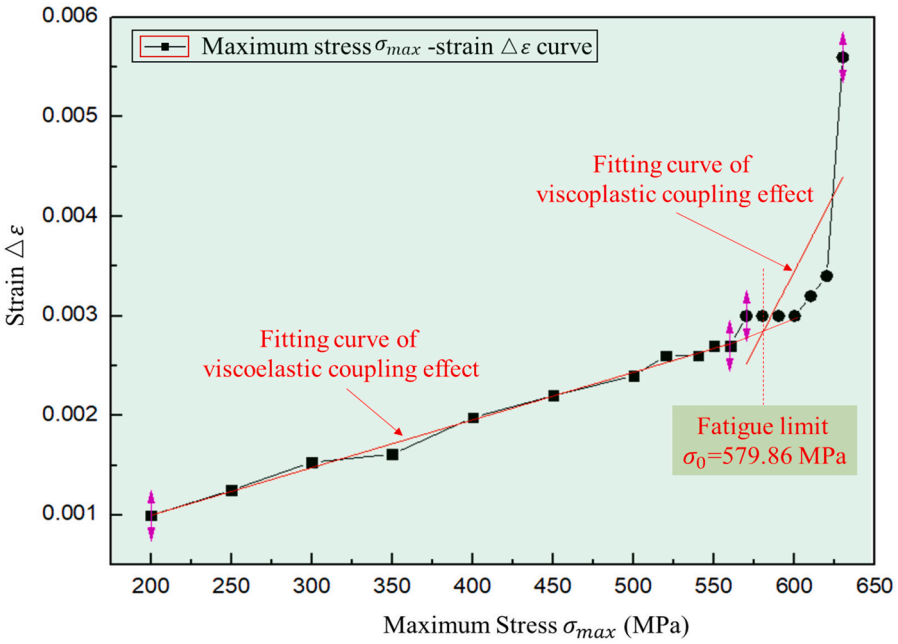

Fig. 10. The relationship between stress and strain under different stress loadings.

Then according to Eqs. (22)–(26), the relationship between the viscous effect of the material and the strain is obtained as follows:

$$\Delta\varepsilon = \frac{40(4.7924 \times 10^{-6})J}{E} \cdot \sigma + 3.8567 \times 10^{-5} \tag{31}$$

Substitute the strain data obtained from the experiment under different stresses into the above equation, the obtained viscosity coefficient J is shown in Table 3. They are obtained from independent experiments on the same specimen under different stresses, so the weighted average of the results in the table shows that the viscosity coefficient J of this material is 5117.7 Pa·s.

Substituting the calculated viscous coefficient J into Eq. (31), the relationship between the viscous effect and strain of 42CrMo4 steel can be obtained as follows:

$$\Delta\varepsilon = (4.8090 \times 10^{-6})\sigma \ + \ 3.8567 \times 10^{-5} \tag{32}$$

According to the energy dissipation theory, the strain change above the fatigue limit mainly comes from the visco-plastic coupling effect. As shown in Fig. 10, The curves with the thermogenesis mechanism of visco-plastic coupling effect were fitted linearly as follows:

$$\Delta\varepsilon = (3.1429 \times 10^{-5})\sigma - 0.0154 \tag{33}$$

Then remove the viscous heat generating part (Eq. (32)) from Eq. (33), as follows:

$$\Delta\varepsilon = (2.6627 \times 10^{-5})\sigma - 0.01544 \tag{34}$$

The above equation is the strain change caused by the plastic effect in the material fatigue experiment. When the plastic strain increment$\Delta\varepsilon = 0$, the calculated stress value σ_0 is 579.86Mpa. It is the fatigue limit of 42CrMo4 steel.

The strain change in Fig. 11 comes from the plastic effect, and the starting point of the plastic effect can be regarded as the fatigue limit of the material. Compared with the fatigue limit value predicted by the Luong method [16], it is found that the difference between the values is 11.8 MPa and the relative error is 2.08 %. Therefore, it is feasible to use the plastic strain increment starting point to predict the fatigue limit.

4.3. Fatigue limit prediction in the local damaged region

In the material fatigue process, damage is the fundamental cause of fatigue failure, and the fatigue failure process is a process of continuous damage accumulation. Fig. 12 shows the strain field at 630 MPa. It can be observed that the distribution of the strain field before fatigue fracture is nonuniform, and the internal dislocations move violently, resulting in a local stress concentration. By comparison with the fractured image, it is observed that the strain concentration region corresponds to the fracture location region of the specimen. This is attributed to the fracture position being located in the damage accumulation region during the fatigue loading process, resulting in a large strain field. Thus, the fracture position of the specimen can be determined according to the change in the

Table 3
Viscosity coefficient calculation data.

Stress	200	250	300	350	400	450	500	520	540	550	560
Strain	9.95e-4	0.00125	0.00153	0.00161	0.00198	0.0022	0.0024	0.0026	0.0026	0.0027	0.0027
viscosity coefficient	5089.1	5156.8	5290.6	4778.0	5165.1	5111.5	5206.0	5242.0	5047.9	5149.6	5057.6

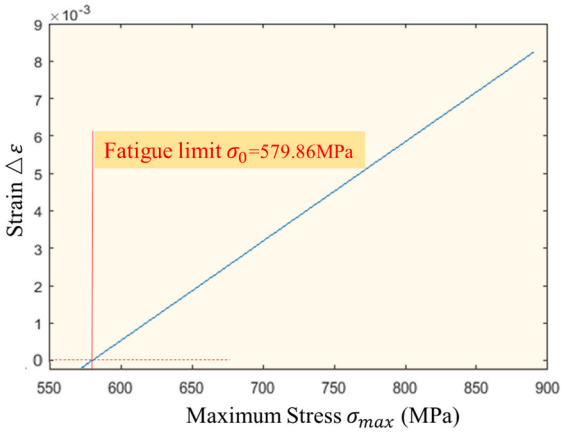

Fig. 11. The relationship between stress and strain under plastic effects.

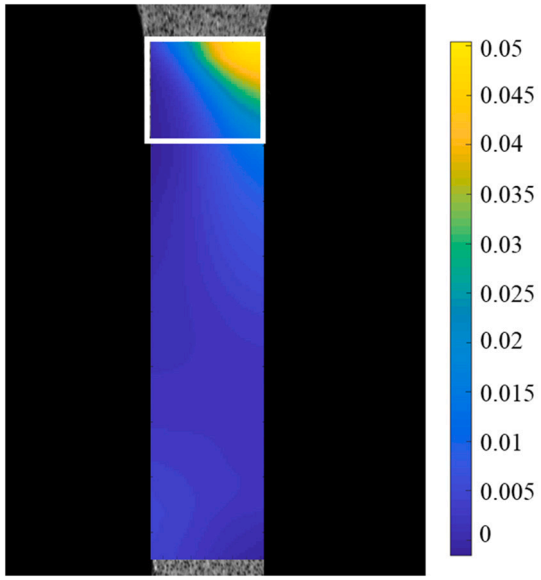

Fig. 12. Strain diagram at 630 MPa.

strain field during the fatigue process. From the perspective of energy dissipation, the local damage location is the point of the highest temperature increase. However, the resolution of the macroscopic measurement scale is insufficient, which conceals a part of the evolution law. Therefore, to strengthen the characteristics, the selection of the calculation region is particularly important in strain calculation. As shown in Fig. 12, the fracture position affects the horizontal direction of the penetrating specimen, which is the width direction of the specimen, and the size is 4 mm. In the vertical direction, the influence range is approximately 3.5 mm. Therefore, the size of the strain calculation region was 4 mm × 3.5 mm, the size of the subregion for the DIC calculation was 29 pixels × 29 pixels, and the step size was 5 pixels.

Fig. 13(a) shows the average strains under different stress loadings in the local damage region. First, the elastic modulus of the local damage region is calculated as 197 GPa using the experimental data, and the viscosity coefficient of the material is obtained as 4918.7 Pa·s using the PSIEDT method. The calculated fatigue limit σ_0 is 572.02 MPa. Fig. 13(b) shows the relationship between the stress in the damage zone and the strain under the plastic effect. Based on Table 4, the PSIEDT method used to predict the fatigue limit provides results similar to those of the commonly used Luong method, and the fatigue limit value obtained using the former for the local damage region is closer to that obtained using the Luong method. The proposed prediction result with the starting point of the plastic strain increment as the parameter has a certain accuracy and applicability.

In addition, in order to verify the rationality of the assumption, especially for the strain caused by the load above the fatigue limit, the following discussion is carried out.

It can be seen from the experimental curves in Fig. 9 and Fig. 13(a) that above the fatigue limit, as the load gradually increases, the specimen appears local plasticity, and the curve is close to nonlinear. Therefore, in order to verify whether the assumptions in this

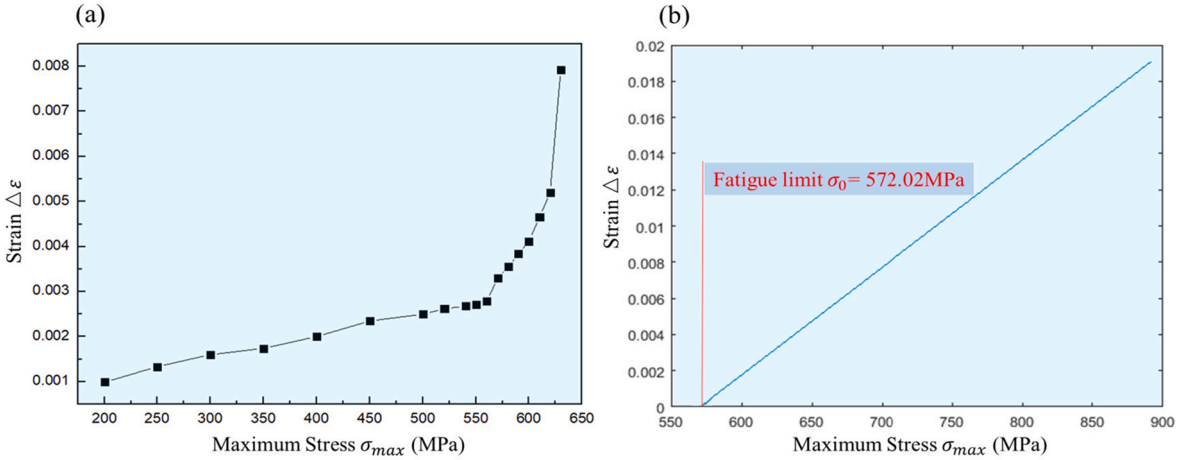

Fig. 13. Fatigue limit obtained by PSIEDT method. ((a) The average strain in the damaged zone under different stress loadings, (b) The relationship between stress and strain under viscoplastic coupling effect).

Table 4
Error analysis of fatigue limit obtained by PSIEDT method.

Method	Luong method	PSIEDT method	Local PSIEDT method
Fatigue limit	568.06 MPa	579.86 MPa	572.02 MPa
Relative error	/	2.08 %	0.70 %

paper is true, the curve below the fatigue limit is linearly fitted, and the curve above the fatigue limit is nonlinear fitting, and the fatigue limit is the stress value at the intersection of the two curves. When performing nonlinear fitting on the curve above the fatigue limit, the power exponent fitting is used here, because the power exponent fitting effect is found to be the best through comparison.

The verification results are shown in Table 5, which shows that the results of the nonlinear fitting calculation of the curve above the fatigue limit are not much different from the results of the approximate linear fitting calculation of the curve. The difference between the results calculated in the entire working region of the specimen and the PSIEDT method is 3.05 Mpa. Compared with the Luong method, the relative error is 2.61 %. And the difference between the calculated results in the local damage region and the local PSIEDT method is only 0.62 MPa. Compared with the Luong method, the relative error is 0.59 %. Therefore, the calculation results are within the margin of error, and the assumptions in this paper are reasonable. For the strain caused by the load above the fatigue limit, it is feasible to do approximate linear fitting.

4.4. Theoretical analysis of the PSIEDT method

Fig. 14(a) shows the strain–temperature rise curve corresponding to the local damage zone. It can be seen that at stage I, the temperature rise of the sample surface first slightly decreases with the increase in the strain and subsequently drops to 0.02 °C when the strain reaches a minimum of 0.16 %. After entering stage II, with the gradual increase in the load, the temperature rise of the sample surface changes from decreasing to increasing. However, the temperature rise rate is low owing to the effect of the low load. Subsequently, at stage III, owing to the further increase in the load, the strain and temperature rise also further increase, and the rising rate tends to be stable. Finally, in stage IV, with the continuous increase in the load, the strain and temperature rise sharply increase until the specimen breaks.

Fig. 14(b) shows the stress–temperature rise and stress–strain curves under different stress loadings in the local damage zone. Based on the energy dissipation theory and the experimental data analysis, we can conclude that stage I is a linear elastic deformation stage. Owing to the thermoelastic effect, the sample surface temperature decreases linearly with increasing stress. After removing the stress loading, the sample completely returns to its original state, and there is no real energy dissipation. After the linear elasticity is exceeded, the sample enters stage II. Owing to the viscoelastic effect, the temperature continues to decrease owing to the increase in the tensile stress, and internal friction is caused by viscoelasticity, which promotes the temperature increase. Consequently, the temperature trend begins to deviate from linear elasticity, and plastic deformation begins, resulting in energy dissipation. This stage is a result of the joint action of elasticity, viscosity, and plasticity. In stage III, the specimen undergoes uniform plastic deformation under the action of stress, and the energy dissipation dominated by plastic deformation also increases uniformly, causing the temperature rise rate to remain substantially constant. In stage IV, the specimen undergoes inhomogeneous plastic deformation, crack propagates, and specimen breaks. Owing to the creation of new surfaces, a large amount of energy is dissipated at the crack tip, causing the temperature of the specimen to increase sharply when fractured. Therefore, this theoretical analysis verifies the reliability of calculating the fatigue limit with the starting point of the plastic strain increment. Thus, it is feasible to analyse and predict the fatigue limit based on the

Table 5
The verification results.

Method	Luong method	PSIEDT method	Local PSIEDT method	Nonlinear fit (above fatigue limit)	
				Entire work region	Local damage region
Fatigue limit	568.06 MPa	579.86 MPa	572.02 MPa	582.91 MPa	571.40 MPa
Relative error	/	2.08 %	0.70 %	2.61 %	0.59 %

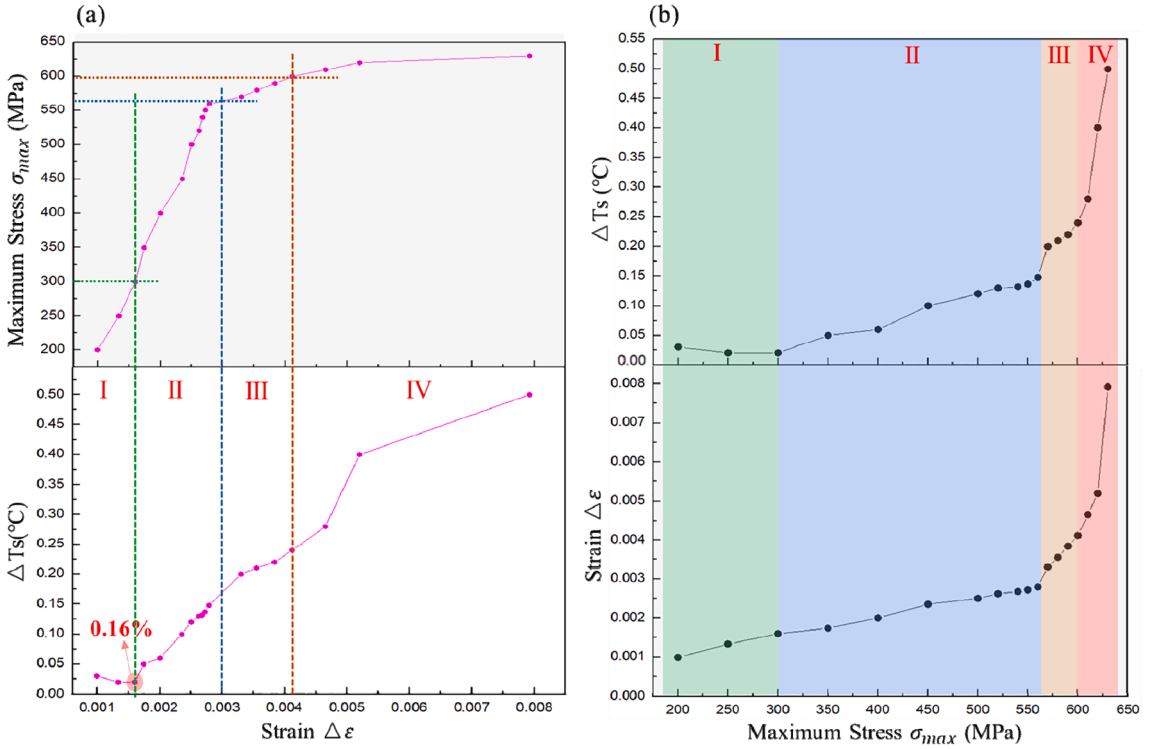

Fig. 14. Theoretical analysis curve of PSIEDT method. ((a) Strain-temperature rise relationship curve in damage zone, (b) The relationship curve between stress and temperature rise and strain).

PSIEDT.

Analysis from a microscopic perspective shows the following. In stage I, at the initial moment, the load is small, and all grains remain intact. After entering stage II, with the gradual increase in the load, dislocations are first generated in the grains, the main dislocations move in the grains, and a few dislocations accumulate near the grain boundaries. The dislocations near the grain boundaries cause micro deformation of the grains, accompanied by an inherent dissipation. In stage III, as the load is further increased, the slip orientations of the grains are also different owing to their different orientations. Many dislocations move to the grain boundaries, accumulating at the grain boundaries, and thereby subjecting the grain boundaries to a large stress concentration. The integrity of the grains is destroyed, and some grains undergo plastic deformation. The inherent dissipation due to deformation also increases gradually. As the load continues to increase, after entering stage IV, the dislocations at the grain boundaries continue to increase, and a corresponding slip occurs, resulting in plastic deformation of all grains and an increase in energy consumption. When dislocations are removed from a grain, cracks grow and a large amount of energy is consumed at the crack tip, causing the specimen to fracture. It can be seen that the starting point of plastic strain corresponds to the transformation of the inherent dissipation mechanism, and the microstructure of the material also changes from reversible to permanent deformation.

4.5. Method advantages

Through experimental verification and theoretical analysis, the method proposed in this paper based on the plastic strain incremental energy dissipation theory (PSIEDT) is feasible to obtain the fatigue limit through the starting point of the plastic strain increment. The main advantages are as follows:

(a) Use fewer samples. Similar to the fatigue thermal imaging method, it is simpler and faster than the traditional experimental method to obtain the fatigue limit and uses fewer samples;
(b) A wider range of applications. When the fatigue limit of metal materials is obtained using the fatigue thermal imaging method, the temperature rise values of some materials that are insensitive to temperature changes are very small. For example, in an experimental test of a nickel-based single-crystal superalloy, the temperature increase did not exceed 0.1 °C until the sample broke. Therefore, the thermal imaging method could not be used to obtain the fatigue limit. The maximum temperature rise of the material used in this study is 0.5 °C, and the resolution of the commonly used infrared camera is 0.1 °C. Specifically, the maximum temperature rise was close to the resolution of the infrared camera, the error was large and was easily affected by the environment. However, the strain measurement accuracy of DIC image correlation technology is more than 100 με, and the plastic strain range of 42CrMo4 steel used in this study is more than 2000 με, which is much higher than its measurement accuracy. Moreover, the strain measurement is not easily affected by the environment. Therefore, this method is more suitable for temperature-insensitive materials compared with infrared thermography.
(c) The theoretical significance is high. In the fatigue thermal imaging method, the Risitano method considers the surface temperature rise as the characteristic response and does not consider the viscoelastic effect. The method ignores that the energy dissipation caused by the viscoelastic effect also causes a temperature change. Although the Luong method [16] considers the temperature change caused by intrinsic dissipation, determining the critical cyclic stress amplitude directly related to the intrinsic dissipation is difficult. The PSIEDT method developed in this study uses the starting point of the plastic strain increment to obtain the fatigue limit from the perspectives of energy dissipation and the heat generation mechanism. The calculation result is similar to that of the Luong method, which has greater theoretical significance.

Notably, while using this method, the acquisition of strain data needs to be focused on. To ensure the accuracy of the experimental results, strain data should be collected once every few fatigue cycles under each stress loading level. To observe the variation in the strain with the fatigue cycle, the variation in strain in the steady state should be selected as the strain data under the stress level. The remaining experimental steps are consistent with those of the fatigue thermal imaging method.

In addition, this method can analyse the deformation and transformation of the energy dissipation mechanism corresponding to the strain and temperature rise inflection point during the fatigue process (the latter is from a microscopic perspective). Therefore, this method has a higher sensitivity and wider applications than temperature measurements because of the limited heat release of many materials.

4.6. Discussions

The method for predicting the fatigue limit proposed in this paper is a deterministic method. That is to say, in the process of predicting the fatigue limit, the applied load, the performance parameters of the material, the geometric parameters of the component and the prediction model are regarded as deterministic values, but in fact these parameters have uncertainties that cannot be ignored. Therefore, aiming at the uncertainty in fatigue limit prediction, the fatigue limit prediction method proposed in this study is analyzed and discussed, which lays a good foundation for further research and reliability evaluation of the method.

There are uncertainties in the production, manufacturing and use of mechanical parts, mainly from: lack of information in the process of production, manufacturing and use; The material properties have strong dispersion; Loads, dimensional effects, service environment, manufacturing accuracy, etc. According to the above situations, the sources of uncertainty in the fatigue limit prediction of materials can be divided into three different types: physical uncertainty, statistical uncertainty, and model uncertainty. According to the fatigue limit prediction method proposed in this paper, considering the influence of the above uncertainties on the fatigue limit, the sources of uncertainty of the components are as follows:

(1) Physical uncertainty. It refers to the natural variation or fluctuation of physical quantities caused by the working environment, experimental procedures, measuring instruments and observers of mechanical parts or materials, resulting in different results when repeatedly observing the same physical quantity. This method mainly includes the loading conditions of the component (loading axial force), the physical change of the material properties of 42CrMo4 (elastic modulus, yield strength, etc.), the geometric size of the component, etc.
(1) Statistical uncertainty. In engineering practice, it is often necessary to collect experimental data, process and save the data, etc. If in these processes, the source of data is uncertain, and the quantity, type and distribution are incomplete, there will be data uncertainty. This method mainly refers to the acquisition and processing of strain data.
(2) Model uncertainty. It mainly comes from the uncertainty caused by idealized assumptions, diversification of theoretical choices or errors in the process of mathematical modeling. Therefore, individual parameters in the model can cause errors in the calculation process. In this method, it is mainly the assumption of the constitutive relationship of materials. In the actual analysis, the model uncertainty can be reduced by improving the model.

Therefore, after the uncertainty analysis of the fatigue limit prediction method proposed in this paper, in order to further test the robustness of the method, its measurement accuracy and stability under different service conditions as well as its applicability to materials with different properties should be studied. In the next research work, the fatigue reliability of components will be modeled and evaluated, so as to further improve the application value of this method in practical engineering.

5. Conclusions

In this study, based on the energy dissipation theory and from the perspective of the fatigue heat generation mechanism, a fatigue limit acquisition method based on PSIEDT was established. Taking 42CrMo4 steel as an example, and relevant experimental and theoretical studies were conducted. The following conclusions were drawn from the analysis of the results:

(1) Based on the energy dissipation theory and the heat generation mechanism of the fatigue process, a PSIEDT was established by combing and understanding the infrared thermal imaging theory. A general relational expression for obtaining the fatigue limit of the material using the starting point of the plastic strain increment was derived.
(2) The fatigue test on 42CrMo4 steel was conducted. Infrared thermal imaging technology and DIC were used to build a fatigue performance test and observation system as well as to set up the corresponding fatigue loading programme. A fatigue limit of 568.06 MPa was obtained using the Luong method in fatigue thermal imaging.
(3) Through the analyses of the strain change and average strains on the sample surface after different stress loadings, it was observed that under low-stress loading, the strain was small. With an increase in the stress, the strain gradually increased, and the specimen underwent permanent deformation until it broke.
(4) Using the PSIEDT method developed in this study, the fatigue limit was 579.86 Mpa, which was 11.8 Mpa greater than that developed using the Luong method, and the relative error was 2.08 %. Therefore, it is feasible to use the starting point of the plastic strain increment to obtain the fatigue limit. By combining the analysis of the surface deformation of the sample with those of the evolution characteristics of the overall strain and strain fields in the local damaged region, it was observed that the energy dissipation in the local damage region was high. Therefore, to further strengthen this feature, the fracture position was selected in the local damaged region to calculate the strain field. The fatigue limit subsequently obtained using the PSIEDT method was 572.02 Mpa, and the relative error versus that using the Luong method result was only 0.70 %. Thus, the developed method is reliable and has relatively high accuracy. If the overall characteristics of the specimen are not evident, this method can be used in the local damage region to obtain the fatigue limit.
(5) According to the energy dissipation theory, the physical relevance of this method was expounded from macroscopic and microscopic aspects. It was concluded that the change in the strain during the fatigue process mainly depends on two mechanisms: non-damage (such as viscoelasticity) and plastic damage mechanisms. The starting point of the plastic strain increment corresponds to the transformation of the two mechanisms. Specifically, the microstructure of the material changes from reversible deformation (viscoelasticity) to permanent deformation (plasticity).

In summary, by theoretical and experimental studies, compared with the fatigue thermal imaging method, this method has the advantage of using few samples, and it adds strain field evolution data, particularly for materials insensitive to temperature. Therefore, this method has a higher sensitivity and more wide applicability than temperature measurements because of the limited heat release of many materials. Therefore, the developed method rapidly obtains the fatigue properties of a material and has high detection accuracy, wide engineering applications, and good practical application prospects.

CRediT authorship contribution statement

Ruili Zu: Writing – review & editing, Writing – original draft, Validation, Methodology, Investigation, Formal analysis, Data curation. **Yingbin Zhu:** Validation, Software, Investigation. **Xianfu Huang:** Supervision, Validation, Data curation. **Yao Huang:** Formal analysis, Methodology, Conceptualization. **Yizhou Zhou:** Formal analysis, Methodology. **Jiaye Zhao:** Conceptualization, Funding acquisition, Methodology. **Zhanwei Liu:** Resources, Project administration, Funding acquisition.

Declaration of Competing Interest

The authors declare that they have no known competing financial interests or personal relationships that could have appeared to influence the work reported in this paper.

Data availability

The data that has been used is confidential.

Acknowledgements

This work was financially supported by the National Natural Science Foundation of China (11972084), and the National Science and Technology Major Project (2017-VI-0003-0073).

References

[1] Zhang J, Liu Z, Sun J, et al. Microstructure and mechanical property of electro pulsing tempered ultrafine grained 42CrMo steel. Mater Sci Engng 2020;782(Apr. 24). 139213.1–139213.10.

[2] Zhang H, Yan X, Hou Q, et al. Effect of cyclic cryogenic treatment on wear resistance, impact toughness, and microstructure of 42CrMo steel and its optimization. Adv Mater Sci Engng 2021.
[3] Shine UP, Nair E. Fatigue failure of structural steel-analysis using fracture mechanics. Proceedings of World Academy of Science Engineering & Technology 2011:631.
[4] Jaroslav P, Roman P, Veronika M. Basic mechanisms leading to fatigue failure of structural materials. Trans Indian Inst Met 2015;69(2):1–6.
[5] Basaran C. Entropy based fatigue, fracture, failure prediction and structural health monitoring. Entropy 2020;22(10):1178.
[6] Zhang W, Jia W, Wen J, et al. Research on Ultra-high Cycle Fatigue Behavior of 42CrMoE Bolt Material for Nuclear Power Station. Heat Working Technology 2018.
[7] Frank H, Frank X. Several common fatigue limit test methods of Metal Materials. Physical and Chemical Test (Physics) 2015;51(06):388–93.
[8] Zhang C. Analysis of Metal Fatigue Performance Based on Thermography. Dalian University of Technology; 2010.
[9] Yu H. Research on rapid evaluation method of fatigue strength and Life based on infrared thermography. Hunan University; 2019.
[10] Xuehui He, Weitao X. Several commonly used fatigue limit test methods for metal materials. Phys Chem Test (Physical Volume) 2015;51(06):388–93.
[11] Pankov AV, Svirsky YA. Experimental investigation of the local deformation processes in joints under cyclic loading by traditional methods of fatigue testing. 2013.
[12] Seite S, Klusák J, Fernándezcanteli A, et al. Comparison of analysis methods of data from thermographic measurements of Al 2024 fatigue limit for R=0.1. 2013.
[13] Guo X. Review of Wang Xiaogang's fatigue thermography research progress in mechanics. Adv Mech 2009;39(2):217–27.
[14] Rosa GL, Risitano A. Thermographic methodology for rapid determination of the fatigue limit of materials and mechanical components. Int J Fatigue 2000;22(1):65–73.
[15] Luong MP. Infrared thermographic scanning of fatigue in metals. Int J Fatigue 1995;19(3):266.
[16] Luong MP. Fatigue limit evaluation of metals using an infrared thermographic technique. Mech Mater 1998;28(1–4):155–63.
[17] Wang X. Life prediction and fatigue analysis based on thermal imaging method. Dalian: Dalian University of Technology; 2009.
[18] Liu H, Zeng W, Ding H, et al. Rapid determination of material fatigue limit using infrared thermal imaging technology. Mech Pract 2007 (04):36–39+54.
[19] Liu H. Experimental study on thermal effect mechanism during fatigue process. Beijing: Beijing University of Chemical Technology; 2007.
[20] Crupi V. An unifying approach to assess the structural strength. Int J Fatigue 2008;30(7):1150–9.
[21] Audenino AL, Crupi V, Zanetti EM. Correlation between thermography and internal damping in metals. Int J Fatigue 2003;25(4):343–51.
[22] Crupi V, Chiofelo G, Guglielmino E. Infrared investigations for the analysis of low cycle fatigue processes in carbon steels. Proc. Institut. Mech. Eng. Part C: J. Mech. Eng. Sci. 2011;225(4):833–42.
[23] Crupi V, Guglielmino E, Maestro M, et al. Fatigue analysis of butt welded AH36 steel joints: Therm graphic method and design S-N curve. Mar Struct 2009;22(3):373–86.
[24] Canteli AF, Castillo E, Arguelles A, et al. Checking the fatigue limit from thermographic techniques by means of a probabilistic model of the Epsilon-N field. Int J Fatigue 2012;39:109–15.
[25] Bremond P, Potet P. Lock-in thermography: A tool to analyze and locate thermomechanical mechanisms in materials and structures. Proc SPIE-Int Soc Opt Engng 2001;4360(1):560–6.
[26] Krapez JK, Pacou D, Gardette G. Lock-in thermography and fatigue limit of metals. In Balageas D, Beaudoin JL, Busse G, et al. (editors.), Proceedings of the 5th international conference on quantitative infrared thermography. Reims: Quantitative Infrared Thermography; 2000, pp. 277–282.
[27] Krapez JC, Pacou D. Thermography detection of early thermal effects during fatigue tests of steel and aluminum samples. In Maldague XP, Rozlosnik AE, (editors.), Proceedings of the 24th International Conference on Thermal Sensing and Imaging Diagnostic Applications. Orlando: International Society for Optical Engineering; 2002, pp. 435–449.
[28] Fan J, Guo X, Wu C. A new application of the infrared thermography for fatigue evaluation and damage assessment. Int J Fatigue 2012;44:1–7.
[29] Fan J, Guo X, Wu C. Influence of heat treatments on mechanical behavior of FV520B steel. Exp Tech 2013.
[30] Fan J, Guo X, Wu C, et al. Research on fatigue behavior evaluation and fatigue fracture mechanisms of cruciform welded joints. Mater Sci Engng A 2011;528(29):8417–27.
[31] Luong M P. Infrared thermographic characterization of engineering materials. In Proceedings of SPIE - The International Society for Optical Engineering 1990;1341.
[32] Luong MP. Infrared thermography of fatigue in metals. Thermosense XIV 1992;1682:222–33.
[33] Chen Y, Sun S, Hong J, et al. Application of digital image technology in deformation measurement of aerospace aluminum alloys. Mater Rev 2016;30(20):144–51.
[34] Chen Y, Sun S, Ji C. Application of three-dimensional digital image correlation technology (3D DIC) in the study of material deformation, progress in application. J Aeronaut Mater 2017;37(4):90–100.
[35] Zou Y. Research on the application of digital image correlation (DIC) method in mechanical properties testing of steel materials. Beijing: Iron and Steel Research Institute 2017.
[36] Favier D, Hervé L, Schlosser P, et al. Homogeneous and heterogeneous deformation mechanisms in an austenitic polycrystalline Ti-50.8 at% Ni thin tube under tension.Investigation via temperature and strain fields measurements. Acta Mater 2007;55(16):5310–22.
[37] Wisner B, Mazur K, Kontsos A. The use of nondestructive evaluation methods in fatigue: A review. Fatigue Fract Engng Mater Struct 2020;43(5):859–78.
[38] Gao H, Liu H, Qi Z, et al. Study on the change law of displacement and strain field at the tip of fatigue crack based on high-speed digital image correlation method. J Military Eng 2015;36(9):1772–81.
[39] Gao H, Liu H, Qi Z, et al. Displacement and strain field measurement of fatigue crack tip based on DIC resonant load. Ordnance Mater Sci Eng 2016;1:16–22.
[40] Duan QY, Li JQ, Li YY, et al. A novel parameter to evaluate fatigue crack closure: Crack opening ratio. Int J Fatigue 2020.
[41] Chrysochoos A, Huon V, Jourdan F, et al. Use of full-field digital image correlation and infrared thermography measurements for the thermomechanical analysis of material behavior. Strain 2010;46(1):14.
[42] Duan QY, Xue HW, Yang YH, et al. Study on fracture behavior of nickelbased single crystal superalloy subjected to high temperature fatigue using digital image correlation. Int J Fatigue 2022;155.
[43] Liu X, Zhang D, Mao C, et al. Full-field progressive fatigue damage of 3D5D braided composites with yarn-reduction: Visualization, classification, and quantification. Compos Sci Technol 2022;218:109214.
[44] Zhou J. Rapid prediction of fatigue limit of 20Cr2Ni4A gear steel based on infrared thermal imaging method. Jiangsu University of Science and Technology; 2019.
[45] Cao D. Research on the fatigue properties of non-ferrous metal materials based on infrared thermal imaging method. Beijing Nonferrous Metal Research Institute 2021.
[46] Liu Y. Research on fatigue properties of ASTM A572 Gr65 steel based on energy dissipation, strain accumulation and microscopic evolution. Taiyuan Engineering; 2021.
[47] Meneghetti G. Analysis of the fatigue strength of a stainless steel based on the energy dissipation. Int I Fatigue 2007;29(1):81–94.
[48] Hopkinson B, Williams GT. The elastic hysteresis of steel. Proc Royal Soc Lond 1912;87:10–7.
[49] Yan Z. Theoretical research on fatigue behavior and evaluation of magnesium alloys and welded joints based on infrared thermal imaging. Taiyuan University of Technology; 2014.
[50] Liu X, Zhang H, Yan Z, Wang W, Zhou Y, Zhang Q. Fatigue life prediction of AZ31B magnesium alloy and its welding joint through infrared thermography. Theor Appl Fract Mec 2013;67:46–52.
[51] Fan J, Guo X, Wu C. Research progress of infrared thermal imaging quantitative analysis method for fatigue characteristics. Mech Pract 2012;36:7–17.
[52] Thomson W. Mathematical and physical papers. London: Focal Press; 1990.

[53] Wei C. Study on fatigue crack propagation behavior of 4003 ferritic stainless steel and its welded joints based on infrared thermal imaging method. Taiyuan University of Technology; 2016.
[54] Farren WS, Taylor GI. The heat developed during plastic extension of metals. Proc Roy Soc A 1925;107:422–51.
[55] Taylor GI, Quinney H. The latent energy remaining in a metal after cold working. Proc Roy Soc A 1934;143:307–26.
[56] Peyroux R, Chrysochoos A, Licht C, et al. Thermomechanical couplings and pseudoelasticity of shape memory alloys. Int J Engng Sci 1998;36(4):489–509.
[57] Mareau C, Fa V, Weber B, et al. Micromechanical modeling if the interactions between the microstructure and the dissipative deformation mechanisms in steels under cyclic loading. Int J Plast 2009;25:106–20.
[58] Kumar SL, Aravind HB, Hossiney N. Digital image correlation (DIC) for measuring strain in brick masonry specimen using Ncorr open source 2D MATLAB program. Results Eng 2019;4:100061.